

A novel transparent conducting MgTiO₃-doped indium oxide thin film and its application for high-performance organic optoelectronic devices

MIAOMIAO TIAN^a, NING WANG^{b,*}

^aCollege of Physics, Changchun Normal University, 677 North Changji Road, Changchun 130032, People's Republic of China

^bSchool of Electrical and Electronic Engineering, Nanyang Technological University, 50 Nanyang Avenue, Singapore 639798, Singapore

A novel transparent conducting oxide, MgTiO₃-doped indium oxide (IMTO), is developed via double source reactive electron beam evaporation technology. The IMTO film exhibits a high work function of 5.16 eV and its stability is demonstrated in air for two months. The optical and electrical properties of IMTO film are also carried out, which are comparable to the commercial ITO. OLEDs and PSCs are fabricated by employing IMTO as anode to try to explore the effects of IMTO on device performance. Due to the outstanding photoelectric characteristics, significant improvements in device performance are achieved for the IMTO-anode OLED and PSC.

(Received August 24, 2015; accepted February 10, 2017)

Keywords: Transparent conductive coatings, Optical materials, Thin film devices and applications, Light-emitting diodes, Polymer active devices

1. Introduction

Over the past few decades, interest in the study of transparent conductive oxides (TCOs) thin films has increased notably. Current progress in transparent conducting oxides (TCOs) is largely driven by the rapid development in the field of opto-electronic devices including flat-panel displays, energy-efficient windows, photovoltaics and organic light-emitting diodes (OLEDs) [1-5]. The performance of such devices is strongly depended on desirable key properties, such as high conductivity, Hall mobility, surface roughness, and transparency of the electrical contacts [6-7]. Therefore, many efforts are currently underway to optimize TCOs to meet various challenges using different approaches that include standard doping as well as the formation of multi-component systems [8]. For instance, efficient hole-injection is essential for obtaining high performance in the case of OLEDs. Nevertheless, efficient hole-injection action is linked to the degree of interfacial hole-injection barrier between anode and hole transport layer (HTL) [9]. Unfortunately, as the most used TCO contact material, indium tin oxide (ITO), has a very low work function ~4.7 eV [10-11]. Generally, large hole-injection barrier can be found between ITO and HTL when ITO is employed as contact anode in OLEDs [12]. This large hole-injection barrier is adverse for device performance as a result of this behavior will results in

poorly balanced charge injection. In order to reduce the energy barrier height for effectively charge carrier transport between ITO and adjacent layer, one of the most commonly ways used is to modify the work function of ITO through the adsorption of organic or inorganic layers [13-17]. However, the inevitable defects generated from fabricating process or post processing can be detected [18-19]. As is known to all, these defects may impair their availability. Therefore, it is of great importance to develop new TCOs with high effective and stable work function to match the energy level of either highest occupied molecular orbital (HOMO) or lowest unoccupied molecular orbital (LUMO) of the molecules for further optimizing the performance for organic optoelectronic devices.

In this paper, we propose a novel TCO, magnesium titanate (MgTiO₃) doped indium oxide (IMTO), with comparable properties in optical and electrical aspects to commercial ITO. Noticeably high work function characteristic of IMTO film is obtained. Typically OLEDs and PSCs are fabricated by employing IMTO as contact anode in regular configuration to demonstrate the effectiveness of work function. Benefiting from the superior photoelectric characteristics of IMTO, the performance of devices with IMTO anode is significantly improved.

2. Experimental details

IMTO thin film was deposited on polished BK7 glass substrates at a substrate temperature of 573 K by double source reactive electron beam evaporation associating with End-Hall IAD (EHIAD) technology. Substrate was kept 35 cm approximately above the center between the two sources. The high-purity source materials, MgTiO₃ granule (5N) and In₂O₃ power (5N) were held in two copper crucibles, respectively. The film deposition rate and thickness were monitored in situ by a commercial vacuum thin film deposition controller (MDC-360C). Two separate mass flow controllers were employed to control the gas flow rate of pure argon and oxygen. The evaporation chamber was initially evacuated at a base pressure of 1.0×10^{-3} Pa, and then argon gas was introduced into the End-Hall ion source and oxygen gas was introduced into the evaporation chamber with a flow rate of 1.5 and 7.5 sccm, respectively. The film was deposited in a reactive oxygen atmosphere which was introduced into the deposition chamber through a calibrated valve at constant pressure $\sim 2 \times 10^{-2}$ Pa. The filament current of electron guns were kept 47 mA and 32 mA corresponded to MgTiO₃ and In₂O₃ crucible sources with constant voltages ~ 8.0 kV. The electrical characteristics of IMTO sample, including room temperature carrier concentration, resistivity and Hall carrier mobility, were carried out by Hall Effect measurements in an 'in house' fabricated sample holder, and the maximum magnetic field applied is 0.55T. The optical transmittance spectra were evaluated with a Shimadzu UV-3101PC spectrophotometer. A GENE SIS2000 XMS 60S (EDAX Inc.) was used to investigate the composition of IMTO film. The surface morphology and root-mean-square (RMS) roughness were performed by using a Digital Instruments Dimension 3100 atomic force microscope (AFM). The surface work function of sample was measured by a KP Technology Ambient Kelvin probe system package.

Using IMTO and commercial ITO thin films as anode contact materials, two OLEDs were fabricated with the following structure: ITO or IMTO/N, N'-bis-(1-naphthyl)-N,N'-diphenyl-1,1Vbiphe-nyl-4,4V-diamine (NPB, 70 nm)/tris(8-hydroxyquinoline)aluminum:10-(2-Benzothiazolyl)-2,3,6,7-tetrahydro-1,1,7,7-tetramethyl-1H,5H,11H-(1) benzopyrpyrano(6,7-8-I,j)quinolizin-11-one [Alq3:C545T(2%), 30 nm]/Alq3 (30 nm)/LiF (1 nm)/Al (150 nm). Similarly, two PSCs employing IMTO and ITO as anodes were also fabricated with the following structure: ITO or IMTO/poly(ethylenedioxythiophene): polystyrene sulphonate [PEDOT:PSS, 20 nm, Clevios P V AI4083]/poly(3-hexylthiophene) (P3HT):indene-C60 bisadduct (ICBA) (~ 190 nm)/LiF (0.8 nm)/Al (150 nm). Apart from the solution processable P3HT:ICBA and PEDOT:PSS layers, other functional layers were deposited under a high vacuum of 5×10^{-4} Pa with a deposition rate about 0.1~0.5 nm/s by thermal evaporation. Current density-voltage-luminance characteristics of OLEDs were measured by employing a Keithley 2400 source meter and a Photo Research PR705 spectra scan system. Current

density-voltage curves of PSCs were performed in a glove box under illumination at 100 mW cm^{-2} using an AM1.5 G solar simulator. The incident light intensity was set at 100 mW cm^{-2} using a NREL calibrated silicon solar cell. Monochromatic incident photon-to-electron conversion efficiency (IPCE) measurements were performed under short-circuit conditions with a lock-amplifier (Stanford Research System, Inc, SR830) at a chopping frequency of 280 Hz during illumination with a monochromatic light from a 150 W Xenon lamp.

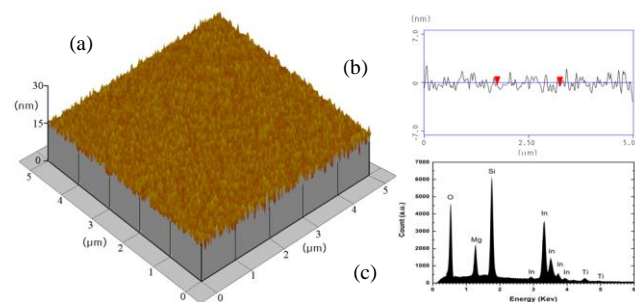


Fig. 1. (a) Characteristics of contact-mode atomic force microscope (AFM) micrographs and (b) the corresponding cross-sectional profile of as-deposited IMTO sample. (c) The EDX spectrum of IMTO thin film deposited on silicon wafer.

3. Results and discussion

3.1. Electrical, optical and elementary content properties

Surface roughness is an important characteristic of TCOs, especially for applications as window electrodes, since TCOs with pinholes or spikes can cause breakdown/shorting, and subsequent upper function layers will undertake the irregular TCOs morphology, adversely influencing performance and stability. Fig. 1a shows AFM image of as-deposited IMTO sample. The surface morphology shows that IMTO sample has a very smooth and uniform surface. Fig. 1b shows that the RMS roughness of sample determined by contact-mode AFM over a $5 \mu\text{m} \times 5 \mu\text{m}$ area is 0.704 nm, which is much smoother than sputter-derived commercial ITO (RMS roughness is about 2.5 nm) [20]. The behavior of smooth and uniform surface properties can be well understood in terms of the process of EHIAD. In this present case, we use End-Hall source to effect film deposition, oxidation, crystallization, and then to result in smooth, dense and coherent IMTO films.

Electrical, optical and elementary content properties of IMTO sample are summarized in Table 1. The energy dispersive X-ray (EDX) results shown in Table 1 are obtained without considering the oxygen present in the film, due to the impossibility of distinguishing between the oxygen signal originating from the silicon substrate and that from the film. The EDX microanalysis is executed at

several random places in the film, and all results exhibit the presence of In, Mg, and Ti (Fig. 1c). The composition of In, Mg, and Ti obtained from the areas of their peaks in the EDX spectra are the same in all these regions for the sample, indicating the uniformity of Mg and Ti dopant distribution in the film. The as-deposited sample harvest a resistivity of $8.1 \times 10^{-4} \Omega \cdot \text{cm}$ with Hall mobility and carrier

concentration of $24.1 \text{ cm}^2 \text{V}^{-1} \text{s}^{-1}$ and $3.2 \times 10^{20} \text{ cm}^{-3}$, respectively, which are fully comparable to that of commercial ITO [21]. Hall measurements indicate that IMTO film is a n-type degenerated semiconductor with carrier concentration in the order of magnitude of 10^{20} cm^{-3} provided by interstitial metal ions or oxygen vacancies [4].

Table 1. Electrical, optical and component properties of the as-deposited IMTO. D : Thickness; ρ : Resistivity; μ : Hall mobility; n : Carrier concentration; \bar{T} : Average transmittance between 400 nm and 1100 nm.

Sample	Element content (Wt. %)			D [nm]	ρ [$\Omega \cdot \text{cm}$]	μ [$\text{cm}^2 \text{V}^{-1} \text{s}^{-1}$]	n [cm^{-3}]	\bar{T} [%]
	In	Mg	Ti					
IMTO	74	17	9	97	8.1×10^{-4}	24.1	3.20×10^{20}	78.9

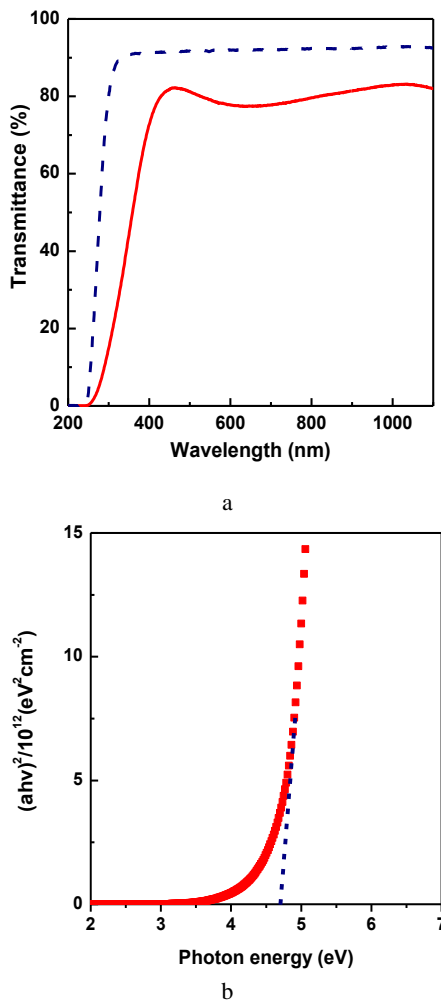


Fig. 2. (a) Transmittance spectra of IMTO thin film (solid line) and the bared BK7 substrate (dash line). (b) The relationship between incident photon energy $h\nu$ and $(ah\nu)^2$ for IMTO sample, the inset dash line shows the optical band gap of IMTO thin film

The UV/VIS/NIR optical transmission spectroscopy of IMTO sample is shown in Fig. 2a. The sample exhibits high transmittance in the VIS/NIR range and a sharp fundamental absorption edge in UV region. It shows that IMTO sample has an average transmittance of better than 78.9% over the spectrum range from 400 to 1100 nm. Considering the factor that the transmittance of bared BK7 glass substrate is only 92% due to reflectivity and absorption losses, the effectively value of IMTO seems to be better attainable. Optical transmission spectra reveal a maximum transmittance of 82.2% at 461 nm wavelength. The visible and near infrared transmittance spectra shows Fabry-Perot oscillations that result from optical interference effect at the air-IMTO and IMTO-substrate interfaces. Below the wavelength of 400 nm, the roll-off transmittance curve results from the onset of band edge absorption. The relation between incident photon energy and absorption coefficient, which can be evaluated from the transmission spectra, is given by

$$(\alpha h\nu)^{1/m} = A(h\nu - E_g) \quad (1)$$

where A is a constant and α is the optical absorption coefficient, E_g is the bandgap energy, m depends on the transitions type [21]. For direct transitions, the value of m is $1/2$, and $3/2$ is for indirect allowed transitions. Hence, the optical band gap for direct transitions can be determined by plotting $(ah\nu)^2$ versus incident photon energy and extrapolating the linear portion of the curves to $(ah\nu)^2 = 0$. While we note that this formalism is not strictly valid for such material, modeling the measured optical spectra with a sharp absorption edge as a direct allowed transition provided a good fit to the data, much better than for assuming an indirect transition. The Fig. 2b shows the plots of $(ah\nu)^2$ versus photon energy ($h\nu$) for IMTO sample. The E_g of the film is estimated to be 4.6 eV, which is larger than the E_g value of indium oxide (~ 3.5 eV). This phenomenon is well known as the

Burstein-Moss shift [22-23].

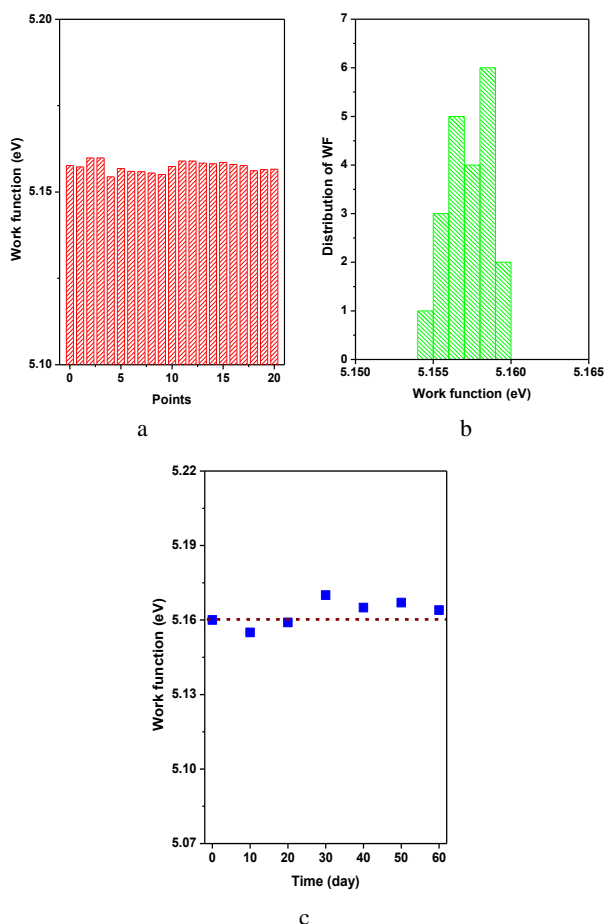


Fig. 3. (a) Work function results of IMTO sample by KP probe. (b) Distribution histogram of work function and (c) it as a function of storage time

Owing to non-contact and non-destructive measurement, the application of Kelvin probe has increased the understanding of surface or interfacial on the nanometer scale [24]. Prior to the measurement of work function for IMTO film, the work function of tip is calibrated by a standard aluminum specimen whose work function is 4.1 eV. As a reference, the work function of commercial ITO sample for 50 points is also carried out (not shown here), which is 4.62 eV and in good agreement with earlier publication result by C. W. Tang et al [25]. The work function results of IMTO film are presented in Fig. 3a. IMTO sample harvests a highly pristine surface work function around 5.16 eV, which is close to the work function of Au (5.2 eV) and much higher than that of commercial ITO. Furthermore, although the number of measurements reach 20, the work function of IMTO sample do not exhibits any substantial change. As complementary expatiation, the histogram distribution of work function versus measuring time is illustrated in Fig. 3b. The obtained values of work function do not vary much and they are centered in 5.16 eV. As shown in the Fig. 3c, the stability of work function is demonstrated.

Although storage time attain two months, the work function of sample is stable. This long-term stability in work function of IMTO provide the potential in commercial applications.

3.2. Effects of IMTO on the performance of OLEDs and PSCs

To illustrate the effects of IMTO on the performance of OLEDs and PSCs, typical OLEDs and PSCs are fabricated by employing IMTO and ITO as contact anodes (Fig. 4a). Fig. 4b-d shows current density-voltage (J - V), current efficiency and luminance characteristics of OLEDs based on IMTO and ITO anodes. As shown, OLEDs with IMTO anode exhibits enhanced performance with maximum luminance and current efficiency of 160900 cd/m^2 and 13.26 cd/A , respectively. It is significantly higher than those (35370 cd/m^2 and 4.8 cd/A) of the ITO-anode device. Moreover, current efficiency of IMTO-anode device do not shows obviously decline even when the current density reaches 1300 mA/cm^2 . On the contrary, current efficiency of ITO-anode device decreases quickly from 4.8 to 2.35 cd/A . Note that the higher current density in Fig. 4a, OLED with the IMTO-anode exhibits a turn-on voltage of 2.20 V which is much lower than 2.91 V of the commercial ITO-anode device. Clearly, the results of IMTO-anode device demonstrate higher electroluminescence performance, which implies that the work function of contact electrode is an important contributing factor on hole-injection barrier in OLEDs [26].

Two bulk heterojunction PSCs utilizing the blend of P3HT and ICBA as photoactive layer are investigated to try to draw meaningfully universal conclusions from direct comparisons of the device performance with different contact anodes. Current density (J_{SC})-voltage curves of the PSCs based on ITO and IMTO anodes are displayed in Fig. 5a. The open-circuit voltage (V_{OC}) of PSCs is verified to be relevant with the difference between HOMO of donor and LUMO of acceptor. In our results, the V_{OC} of PSCs with ITO and IMTO anodes have the same value of 0.82 V. However, the PSC based on IMTO anode shows superior power conversion efficiency (PCE) value of 6.03% with a J_{SC} of 10.74 mA/cm^2 and a fill factor of 68.5% when the ITO device exhibits a moderately reduced PCE value of 5.56% with a J_{SC} of 10.36 mA/cm^2 and a fill factor of 65.4%. The main distinction in device performance lies in short-circuit current density and fill factor which are closely linked to the suppressed charge recombination, fine nanostructure morphology of active layer, and contact electrodes [27]. On account of the same preparation condition for active layers, the smoother surface and higher work function of contact anode should contribute positive factors for enhanced performance of PSCs. Figure 5b show the external quantum efficiency (EQE) curves of devices based on various anodes. It is identified that the J_{SC} measured from devices are well consistent with integrated values (10.82 and 10.21 mA/cm^2 for IMTO and

ITO based devices, respectively) of the EQE spectrum.

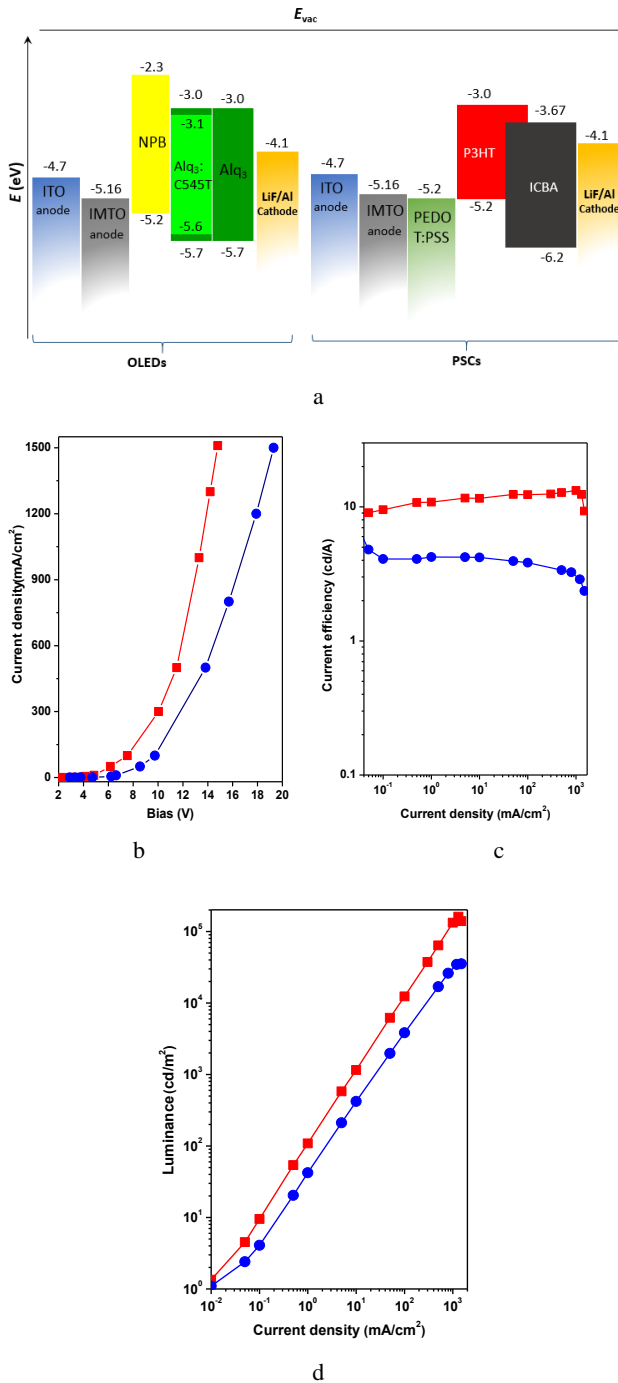


Fig. 4. (a) Device architectures and energy level diagrams of OLEDs and PSCs used here. (b) Current density-bias, (c) current efficiency-current density and (d) luminance-current density curves of the OLEDs with different contact anodes. The solid lines with square and circle represent the devices with IMTO and ITO anodes, respectively

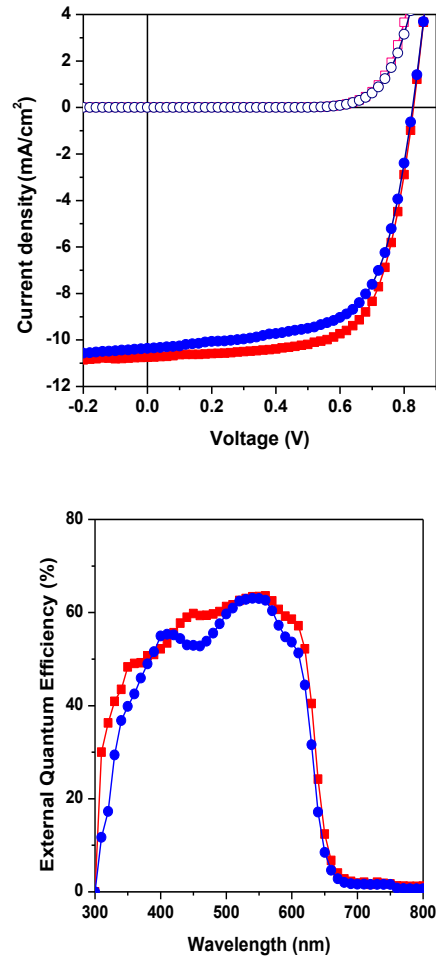


Fig. 5. (a) Current density (J_{SC})-voltage (V) curves without and with illumination under an AM 1.5G solar simulator of PSCs based on different anodes. (b) The corresponding external quantum efficiency curves for (a). Curves of IMTO-anode and ITO-anode PSCs are represented by the lines with square and circle, respectively

4. Conclusion

We have successfully developed a novel high work function transparent conducting oxide-MgTiO₃ doped indium oxide-by EHIAD technique. The IMTO film exhibits highly competitive optical and electrical characteristics comparing with the commercial ITO [28-29]. Direct optical bandgap of 4.60 eV and high work function of 5.16 eV for IMTO are obtained. Furthermore, the stability of work function is demonstrated. The effects of IMTO thin film on the performance of OLEDs and PSCs are determined. The turn-on voltage of OLEDs show obviously decline from 2.91 to 2.20 V when we apply IMTO to replace commercial ITO as contact anode. Furthermore, the luminance and current efficiency are steady improved in the IMTO-anode OLED and the enhancement in PCE by 10% is accomplished in the PSCs

with IMTO as anode. The significant improvements in device performance should be attributed to a combination of small surface roughness, high work function and excellent optical and electrical properties of IMTO. Our results reveal that IMTO is an alternative TCO material for high-performance organic optoelectronic devices and can be widely applied in other fields as energy-efficient window.

Acknowledgments

This work was financially supported by Jilin Provincial Education Department (Grant No. 2013-257, 2014-260) and the National Natural Science Foundation of China (NSFC, Grant No. 61404010).

References

- [1] J. L. Vossen, *Phys. Thin Film* **9**, 1-72 (1977).
- [2] C. W. Tang, S. A. VanSlyke, *Appl. Phys. Lett.* **51**, 913 (1987).
- [3] T. J. Coutts, D. L. Young, X. N. Li, *MRS Bull.* **25**, 58 (2000).
- [4] P. P. Edwards, A. Porch, M. O. Jones, D. V. Morgan, R. M. Perks, *Dalton Trans.* **19**, 2995 (2004).
- [5] C. W. Tang, *Appl. Phys. Lett.* **48**, 183 (1986).
- [6] R. X. Wang, A. B. Djuricic, C. D. Beling, S. Fung, (Nova Science Publishers, Inc., New York, 2005), Chap. 6.
- [7] D. S. Ginley, C. Bright, *MRS Bull.* **25**, 15 (2000).
- [8] T. Minami, *Semicond. Sci. Technol.* **20**, 35 (2005).
- [9] W. Chen, C. Huang, X. Y. Gao, L. Wang, C. G. Zhen, D. Qi, S. Chen, H. L. Zhang, K. P. Loh, Z. K. Chen, A. T. S. Wee, *J. Phys. Chem. B* **110**, 26075 (2006).
- [10] F. Cacialli, J. S. Kim, T. M. Brown, J. Morgado, M. Granstrom, R. H. Friend, G. Gigli, R. Cingolani, L. Favaretto, G. Barbarella, R. Daik, W. J. Feast, *Synth. Met.* **109**, 7(2000).
- [11] V. Adamovich, S. R. Cordero, P. I. Djurovich, A. Tamayo, M. E. Thompson, B. W. D'Andrade, S. R. Forrest, *Org. Electron.* **4**, 77 (2003).
- [12] N. Koch, S. Duhm, J. P. Rabe, *Phys. Rev. Lett.* **95**, 237601 (2005).
- [13] N. Koch, A. Kahn, J. Ghijsen, J.-J. Pireaux, J. Schwartz, R. L. Johnson, A. Elschner, *Appl. Phys. Lett.* **82**, 70 (2003).
- [14] D. J. Milliron, I. G. Hill, C. Shen, A. Kahn, Schwartz, J. J. *Appl. Phys.* **87**, 572 (2000).
- [15] K. Sugiyama, H. Ishii, Y. Ouchi, K. Seki, *J. Appl. Phys.* **87**, 295 (2000).
- [16] F. Nüesch, L. J. Rothberg, E. W. Forsythe, Q. T. Le, Y. Gao, *Appl. Phys. Lett.* **74**, 880 (1999).
- [17] S. Khodabakhsh, D. Poplavskyy, S. Heutz, J. Nelson, D. D. C. Bradley, F. Murata, T. S. Jones, *Adv. Funct. Mater.* **14**, 1205 (2004).
- [18] M. P. Jong, L. J. Ijzendoorn, M. J. A. De Voigt, *Appl. Phys. Lett.* **77**, 2255 (2000).
- [19] W. H. Kim, A. J. Mäkinen, N. Nikolov, R. Shashidhar, H. Kim, Z. H. Kafafi, *Appl. Phys. Lett.* **80**, 3844 (2002).
- [20] Y. Yang, Q. Huang, A. W. Metz, J. Ni, S. Jin, T. J. Marks, M. E. Madsen, A. Divenere, S.-T. Ho, *Adv. Mater.* **16**, 321 (2004).
- [21] I. Hamberg, C. G. Granqvist, *J. Appl. Phys.* **60**, R123-R159 (1986).
- [22] E. Burstein, *Phys. Rev.* **93**, 632 (1954).
- [23] T. S. Moss, *Proc. Phys. Soc. Lond. Soc. B* **67**, 775 (1954).
- [24] M. Nonnenmacher, M. P. O'Boyle, H. K. Wickramasinghe, *Appl. Phys. Lett.* **58**, 2921 (1991).
- [25] Y. Park, V. Choong, Y. Gao, B. R. Hsien, C. W. Tang, *Appl. Phys. Lett.* **68**, 2699 (1996).
- [26] Y. Yang, E. Westerweele, C. Zhang, P. Smith, A. J. Heeger, *J. Appl. Phys.* **77**, 694 (1995).
- [27] G. Li, R. Zhu, Y. Yang, *Nat. Photon.* **6**, 153 (2012).
- [28] K. H. L. Zhang, Y. Du, A. Papadogianni, O. Bierwagen, S. Sallis, L. F. J. Piper, M. E. Bowden, V. Shutthanandan, P. V. Sushko, S. A. Chambers, *Adv. Mater.* **27**, 5191 (2015).
- [29] X. Yu, T. J. Marks, A. Facchetti, *Nat. Mater.* **15**, 383 (2016).

*Corresponding author: ning_wang@outlook.com